Solar Energy 285 (2025) 113093

Contents lists available at ScienceDirect

Solar Energy

journal homepage: www.elsevier.com/locate/solener

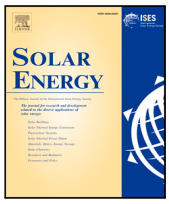

Design, construction, and qualification of a lightweight, modular heliostat made from high-performance concrete

Patrick Forman [a,*], Marius Schellen [b], Tim Schlichting [c], Andreas Pfahl [d], Peter Mark [a], Christian Glock [b], Jürgen Schnell [b]

[a] Ruhr University Bochum, Institute of Concrete Structures, Universitätsstraße 150, 44780, Bochum, Germany
[b] University of Kaiserslautern-Landau (RPTU), Concrete Structures and Structural Design, Paul-Ehrlich-Straße, Building 14, 67663, Kaiserslautern, Germany
[c] DLR, German Aerospace Center, Institute of Solar Research, Qualification, Karl-Heinz-Beckurts-Str. 13, 52428, Jülich, Germany
[d] DLR, German Aerospace Center, Institute of Solar Research, Solar Power Plant Technology, Karl-Heinz-Beckurts-Str. 6, 52428, Jülich, Germany

ARTICLE INFO

Keywords:
Heliostat
Solar thermal collector
Concrete construction
Modular construction
Qualification
Photogrammetric measurement

ABSTRACT

With regard to climate change and the importance of utilization of solar energy, the development of a modular concrete heliostat is presented. The focus thereby lies on the design and the construction of the concentrator structure, demonstrating the technical proof of concept for a small-scale collector. The idea of using concrete as a structural material is its free shapeability, and its worldwide availability. With respect to accuracy demands, a high-performance concrete (HPC) is used that possesses a high compressive and also tensile strength. The collector is designed as a strut-like structure with main radial beams and a central mount to ensure high stiffness. A circular design minimizes shading effects in the solar field. By employing symmetry reduction methods, the concentrator is dissolved into equal segments making it a modular construction. To demonstrate the feasibility, a prototype with diameter 3.2 m and a weight of just about 340 kg consisting of four modules was developed. The production is achieved using a modular formwork made from polystyrene at the RPTU Kaiserslautern. The concrete heliostat is built-up and qualified at the solar tower Jülich (Germany) by means of photogrammetric measurement of the mirror surface. In addition, the concrete structure was measured in the lab of the Ruhr University Bochum. The deformations of the concrete structure vary mainly in the range of ±1 mm only indicating remarkable stiffness. In contrast, the mirror deformations reveal an optical efficiency of $SDrms = 7.8$ mrad. However, these deformations are primarily attributed to the simple mirroring concept by means of clamping, which was not the central subject of the development. However, deviations between varying collector positions are less than 2 mm and only occur in local areas of single mirror facets, which additionally underlines the stiffness of the concrete structure.

1. Introduction

The installed capacity of concentrated solar power (CSP) plants exhibits more than 6 GW with an additional 1.5 GW under construction in 2021 [1]. However, photovoltaic (PV) technology is currently more mature and widely used due to its lower costs. Yet, CSP becomes more important concerning ongoing climate change and the targeted replacement of fossil energy consumption to achieve a CO_2-neutral energy supply in the coming years or decades [2]. Additionally, it exhibits a higher efficiency than PV [3]. In CSP plants, the incoming direct solar radiation is concentrated onto a receiver using mirrored

Abbreviations: A_r, reflecting area; c_{pe}, wind load coefficient; C_i, force or moment coefficient; CSP, concentrated solar power; CST, central solar tower; d, diameter of the heliostat; E_{cm}, mean Young's modulus of concrete; f, focal length; f_{cm}, mean compressive strength of concrete; f_{ctd}, design value of concrete's tensile strength; f_{ctm}, mean tensile strength of concrete; $f_{ctm,fl}$, mean flexural tensile strength of concrete; f_{yk}, yield strength of reinforcement; F_x, horizontal wind force; F_z, vertical wind force; FE, finite element; GWP, global warming potential; h, height; h_{beam}, cross-section height of the beam; HPC, high-performance concrete; I_r, moment of inertia in radial direction; l, length; M_{hy}, hinge moment; n, shape coefficient; NC, normal-strength concrete; P_r, circular line-like load; PTC, parabolic trough collector; PV, photovoltaic; q_{ref}, reference wind pressure; q_b, basic wind load; q_w, wind load; R, radius; RMS, root mean square; SD, slope deviation; $SDrms$, RMS of the slope deviation; $SDrms_{cs}$, RMS of the concrete structure's slope deviation; $SDrms_m$, RMS of the concrete mirror facet's slope deviation; ULS, ultimate limit state; v_{ref}, reference wind speed; α, pitch angle (tilting axis); β, yaw angle (direction of wind or rotation axis); γ_c, specific weight of concrete; ν, Poisson's ratio; ρ, air density; ρ_c, bulk density of concrete; σ_c, concrete's stress; ϵ_c, concrete's strain; φ, angle of a modular segment

* Corresponding author.
E-mail address: patrick.forman@rub.de (P. Forman).

https://doi.org/10.1016/j.solener.2024.113093
Received 5 October 2023; Received in revised form 11 October 2024; Accepted 7 November 2024
Available online 28 November 2024

collectors. Thereby, a heat transfer fluid is heated up so that electricity can be generated by means of a conventional turbine. If heat storage is integrated, electricity can also be harvested when no direct solar energy is available. This denotes the main advantage of CSP in contrast to PV, where direct and indirect solar energy is directly transferred into electricity. The most established CSP systems are parabolic trough collectors (PTC), which are also the most cost-effective [4,5]. However, central solar tower (CST) plants can achieve higher temperatures of up to about 700-1000 °C, in contrast to about 400 °C for PTC, due to a higher concentration ratio of solar radiation. Therefore, a multitude of collectors, called heliostats, are arranged in a solar field to point-wise concentrate the solar radiation onto a receiver arranged on a solar tower by means of rotationally symmetrical parabolic shaped mirrors. Hence, they are seen to be the most promising CSP technology in the next years [6].

Current trends in CSP aim for cost reduction to be competitive on the market, especially for CST systems [7–11]. Hereby, developments on the level of the solar field, e.g. solar field layout [12–14], hybrid plants [15,16], or receiver type [17], and also of the heliostat, e.g. structural design [7,18–21], or wind loads [8,22–24], are part of the evolution to be able to attain holistic advancement. On the structural level of heliostats, T-shaped heliostats with glass mirror facets have become the most widely used technology for heliostat structures [7]. However, due to the separation between the pylon with the torque beam forming the typical T-shape, and a rectangular concentrator consisting of additional cross beams that support the mirror facets, the deformations of these subsystems superimpose. In [20], a T-shaped heliostat with an umbrella-like supporting structure is therefore introduced to stiffen the structure. In contrast, the Stellio heliostat [25,26] possesses a central mount with main radial beams as a steel framework and exhibits a pentagonal shape of the mirror area. Since the load path is thereby reduced, its design is materially simplified and exhibits great accuracy, serving as a benchmark in this article. Other designs aim for the minimization of wind loads since they are crucial for the design, e.g., a lay-down heliostat [27]. It is designed as a sandwich structure made from aluminum with a soft core, featuring radial main bearing elements and an almost circular shape. In addition, it has been shown that circular or polygonal shapes of concentrators minimize shading between individual collectors, enabling a denser distribution in the solar field, which means that more mirror surfaces can be used [28]. The first known heliostat made from concrete, due to its cheap material, is demonstrated, among various others, in [8]. It consists of a massive concentrator structure with thicknesses in the range of decimeters and needs an equally weighted counterweight for the bearing in its centroid, which is by no means a resource-efficient design. However, for PTC, it could be shown that thin shells made from high-performance concrete (HPC) are a promising alternative to conventional steel framework collectors [29,30]. Based on the developments on PTC, the shell-like structure is now to be dissolved into a strut-like structure increasing the statical height of the cross-section and therefore the stiffness for heliostats.

In the article, the conceptual design for heliostats made from HPC is derived. For the design, symmetry reduction methods lead to a grillage structure for the concentrator. A rotationally symmetrical, modular structure is thereby derived [31]. The design is constrained by accuracy demands and stress limits of the used concrete. The action effects, mainly dead and wind loads, are considered for both, operational and survival state. The manufacturing of a heliostat prototype and its construction at the solar field in Jülich (Germany) is presented. The substructure of the prototype, originally part of a former steel heliostat, has been adapted for the concrete structure, including the extension of the substructure for a central mounting. By means of photogrammetric measurement of the mirror surface as well as of the concrete structure itself, the optical quality of the mirroring and the geometrical stability of the grillage is evaluated. The focus lies on the derivation of a modular concrete concentrator as a technical feasibility study in small scale. Further investigations, especially in terms of cost reduction and economic comparability with other concentrator systems are subject of further research.

2. Design of modular concrete heliostats

2.1. Geometry of the mirror surface

The mirror surface of solar thermal collectors is of parabolic shape for solar concentration. Vertically incident solar rays are reflected and thereby focused in the focal point that is defined by the focal length f. Heliostat's mirrors hence have to exhibit a rotationally symmetrical parabolic shape for a pointwise concentration. The course of the height z is given by the parabolic function in Eq. (1).

$$z(r) = \frac{1}{4f} r^2 \tag{1}$$

Here, r represents the radius of a paraboloid and f corresponds to the distance between reflector and receiver.

Although a paraboloid shape is not essential for heliostats, as they are not aligned with the axis of irradiation for solar concentration, a classic spherical shape – which would have been easier to implement – was deliberately avoided. Instead, the paraboloid shape was chosen to showcase the versatility and free formability of concrete.

2.2. Conceptual design

The conceptual design of heliostats made from HPC aims to fulfill both, a lightweight structure and a high stiffness [32]. For PTC, concrete shells with directly glued mirror foil, which do not possess remarkable stiffness, provide a merged bearing structure and geometrically stable, areal support for the mirroring surface [33]. In contrast to PTC, the accuracy demands for heliostats are enhanced since the focal length increases from 2–3 m to several hundred meters. To gain the stiffness, an increased cross-section height perpendicular to the direction of loading of the concrete structure is required, as the impact of height on the moment of inertia is exponential. To reduce material consumption while ensuring low deformations, the concrete concentrator is conceptually designed as a grillage. However, now also the mirror elements themselves need enough stiffness to overbridge the gaps of the grillage.

Generally, the concentrator is defined by a grillage structure with an outer circular shape. Due to the circular shape, shadowing effects in the solar field are minimized allowing a dense field layout. Also, the concentrator structure can be segmented into single modules represented as "slices of cake". With respect to the number of heliostats used in a CST system, the number of identical modules increases additionally due to the segmentation. This make a serial production of precast concrete parts more viable [34]. Ensuring proper quality management in the production, the required accuracy can be directly controlled in prefabrication. Fig. 1 shows the design at the example of the prototype to be built that consists of four (almost) equal concrete modules for the concentrator. It exhibits a central mount by means of an inner steel ring where the concrete modules are attached. The main bearing elements are radial beams that reduce the load path of the structure. This design is similar to the Stellio heliostat [26]. An outer ring defines the circular shape, secondary struts transfer the loads and serve as additional support for the mirror elements. In addition, Fig. 1 shows the substructure consisting of a steel pylon with a traverse and especially designed C-shaped steel suspensions for the central mount.

The geometric dimensions of the prototype are defined by a diameter of 3.2 m, whereby a focal length of $f = 92$ m is assumed. Thereby, the curvature of the reflector is defined by a height of 7 mm at the edge at $r = 1.6$ according to Eq. (1). The height of the tilting axis from the ground is 2.4 m so that a maximum total height with an assumed deflection of 0° – morning position – results to 4 m. The reflecting area is $A_r = 8.04\,\mathrm{m}^2$, which characterizes the prototype as a small-scale collector.

Table 1
Material properties of the HPC based on the binder Nanodur compared to a NC (m - mean value).

Description		HPC	NC (C30/37)	Unit
Young's modulus	E_{cm}	47,500	33,000	MPa
Poisson's ratio	ν	0.20	0.20	–
Compressive strength	f_{cm}	116	38	MPa
Flexural tensile strength	$f_{ctm,fl}$	20	5.8	MPa
Axial tensile strength (design value)	f_{ctd}	6.6	1.1	MPa
Bulk density	ρ_c	2500	2500	kg/m^3
Global warming potential	GWP	460	219	kg CO_{2e}/m^3

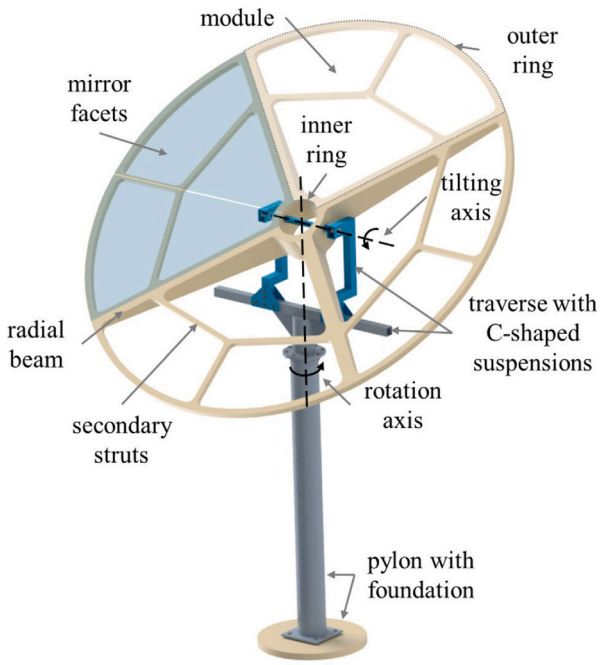

Fig. 1. Conceptual design of a strut-like, modular concrete heliostat.

2.3. High-performance concrete

Concrete usually has high compressive strength f_c but quite low tensile strength f_{ct}. If f_{ct} is exceeded, brittle failure occurs. To avoid this, concrete structures exhibit reinforcements in their tensile areas that ensure ductile component behavior. However, until the tensile strength is reached, concrete behaves linear-elastic according to Hook's law:

$$\sigma_c(\varepsilon_c) = E_c\varepsilon_c \quad \text{for} \quad 0 \le \sigma_c \le f_{ct} \tag{2}$$

Herein, σ_c and ε_c correspond to the concrete's stress and strain, respectively, while E_c assigns its Young's modulus.

When the first crack occurs, the tensile stresses are transmitted to the reinforcing steel and a softening, non-linear deformation behavior occurs. In compression, normal-strength concrete (NC) exhibits an almost linear elastic behavior up to 40% of its compressive strength f_c. But for HPC or ultra-high-performance concrete (UHPC) this applies up to 80%–90% of f_c. To ensure the lowest possible deformations for solar collectors, the aim of the design is to keep an uncracked structure. This means that tensile stresses must be kept well below f_{ct}.

For the manufacturing of concrete heliostats, an HPC based on the binder Nanodur Compound 5941 is proposed, which – in addition to its high durability, its good workability, and its self-compacting behavior – is characterized by high compressive and tensile strength as well as Young's modulus that is approximately 1.5 times greater than that of NC. Hence, for a low-deformation structure, the tensile strength and the Young's modulus are of particular importance (cf. Eq. (2)), as these mainly determine the deformations. The essential parameters for the design are summarized in Table 1 in comparison to a NC of class C30/37. In addition, the carbon footprint, by means of the global warming potential (GWP) defined by the equivalent CO_2-emissions per volume from production, is listed to support environmental analysis. More detailed information as well as the concrete mix are given in [33].

The Young's modulus used for the design – incorporating all analytical and numerical derivations – is set to 47,500 MPa. The mean flexural tensile strength is determined to $f_{ctm,fl} = 20$ MPa in 3-point bending tests made at the structural testing laboratory of the University of Kaiserslautern-Landau (RPTU) using prisms with dimensions of $l/h/b = 160/40/40$ (mm) according to applicable standards [35,36]. To ensure linear-elastic behavior, the first principle stress must be limited to the design value of the axial tensile strength. Therefore, the mean flexural tensile strength is first transferred to the mean axial tensile strength and second, the characteristic 95%-quantile value is calculated based on the scattering data of the tests. In addition, the characteristic value is reduced by partial safety factors as described in [33] so that the reduced axial tensile strength follows to $f_{ctd} = 6.6$ MPa for the design. Furthermore, the self weight of the (reinforced) concrete is given by the averaged bulk density of 2500 kg/m^3. Compared to NC, the HPC possesses about twice as much GWP. However, since the strength of the HPC is up to six times higher, a structure made from NC would need much more material and thus yielding a higher GWP in total. Also similar high-performance concretes exhibit a GWP of 767 kg CO_{2e}/m^3 [37] which is even higher than the one used here. In contrast, (reinforcing) steel has a carbon footprint of 4426 kg CO_{2e}/m^3.

It must be noted that the costs for HPC are generally higher than for NC. But, to achieve such slender designs as derived here, NC is inappropriate since it would require much thicker dimensions. These again cause higher dead loads since the bulk densities of both materials are equal, which affect the dimensions of the foundation, the drive system and the concentrator structure itself.

2.4. Specific action effects

The specific effects on heliostats mainly comprise dead and wind loads. Wind loads are affected by the deflection of the collector. Dead loads cause varying internal forces in the structure during sun tracking. Wind loads in particular strongly depend on the shape of the heliostat and, consequently, the wind flow around it [38,39]. For design, distinction is made between two essential states, namely the operating and the survival one:

- In the operating state, the collector tracks the sun under moderate mean wind speeds at elevation axis height of up to 10 m/s in such a way that the solar rays are focused on the receiver in the solar tower. This corresponds to a peak wind speed of 20 m/s at 10 m height.
- In the survival state, under hurricane-like mean wind speeds of up to 33 m/s at elevation axis height, the collector is fixed in stow position at a deflection of 90° – mirror facets directed upwards – and no operation takes place. This corresponds to a peak wind speed of 65 m/s at 10 m height.

Table 2
Wind load coefficients for parabolic dish collectors according to [41] with adjusted denotations according to Fig. 2.

	Operation			Stow
α [°]	0	60	30	90
β [°]	0	0	180	0
C_{Fx}	3.5	1.9	−1.8	0.33
C_{Fz}	0.31	3.1	0.8	0.98
C_{MHy}	0.31	0.25	0.35	0.22

Dead loads arise from the reinforced concrete structure itself as well as the mirror facets and their fasteners. The concrete used including reinforcement is taken into account by the averaged bulk density (cf. Table 1). The weight of the mirror elements depend on the type used. Here, the ALMECO *vegaPrime* type with a total thickness of 2 mm is considered. It is built up as a composite consisting of two outer layers made from aluminum with a thickness of 0.5 mm and a plastic core. This results in a weight of 2.9 kg/m^2 [32].

The wind loads on the heliostat can be determined by means of wind load coefficients c_{pe}. These coefficients describe the wind pressure distribution over the mirror surface of the heliostat's concentrator. Multiplied with the reference pressure q_{ref} – depending on the reference wind speed v_{ref} and the air density $\rho = 1.25\,\mathrm{kg/m^3}$ – the wind load q_w results:

$$q_w = c_{pe}\, q_{ref} \tag{3}$$

with:

$$q_{ref} = \frac{1}{2}\rho v_{ref}^2 \tag{4}$$

Thereby, q_{ref} results to 0.06 kN/m^2 for the operation state with maximum mean wind speed at elevation axis height of $v_{ref} = 10\,\mathrm{m/s}$, and to 0.68 kN/m^2 for the survival state with a maximum mean wind speeds at elevation axis height of $v_{ref} = 33\,\mathrm{m/s}$, respectively.

For the design of the concrete concentrator, deflection-related wind load coefficients c_{pe} were adapted from wind tunnel tests in [40]. Here, the distributions of c_{pe} are derived for different positions of the concentrator with respect to the pitch angle α (tilting axis) and yaw angle β (direction of wind or rotation axis, respectively). It must be noted that the c_{pe} coefficients are valid for rectangular-shaped concentrators only, but are simplified to the circular shape here.

For the design of the substructure consisting of the pylon, traverse, and suspensions for the central mount, force and moment coefficients C_i were adapted from the wind tunnel tests at parabolic dishes in [41]. By means of the aforementioned reference wind pressure q_{ref} as well as the geometric dimensions of the concrete heliostat, the characteristic attacking forces and moments can be calculated to:

$$F_x = C_{Fx} \cdot q_{ref} \cdot A_r \quad \text{(horizontal force)} \tag{5}$$

$$F_z = C_{Fz} \cdot q_{ref} \cdot A_r \quad \text{(vertical force)} \tag{6}$$

$$M_{Hy} = C_{MHy} \cdot q_{ref} \cdot A_r \cdot d \quad \text{(hinge moment)} \tag{7}$$

Here, C_{Fx}, C_{Fz}, and C_{MHy} are the respective force and moment coefficients, F_x, F_z, and M_{Hy} the corresponding forces and moment (Fig. 2), A_r is the reflecting surface, and d is the diameter of the parabolic dish or heliostat, respectively. The assumed wind load coefficients according to [41] for the decisive deflection in the operational state and stow position are summarized in Table 2.

It must be noted that the values are derived for parabolic dishes with a depth-to-diameter ratio of 0.1. In contrast, the planned prototype possesses a ratio of 0.002, which is comparatively high for heliostat concentrators. Due to this geometrcial simplification, an enhanced partial safety factor of 2 is assumed increasing q_w for the design and detailing of the substructure and also for the concentrator.

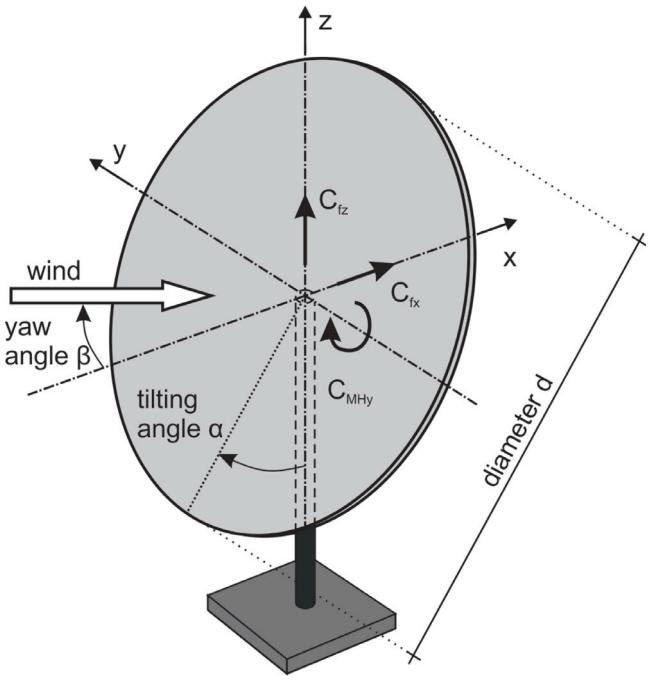

Fig. 2. Coordinate system for solar collector with wind coefficients following.

However, for concrete collectors, it has been shown that a horizontal collector position (90°) becomes decisive for both states, operational as well as survival state, since the dead load dominates here [32,33]. It must be noted that in the operational state a horizontal position is not reached, since it is not necessary for focussing the solar radiation on the receiver. For the design, the 90° position is used in survival but also operational state for the sake of simplicity.

2.5. Accuracy demands

The (optical) efficiency mainly depends on maintaining an undisturbed mirror surface. However, due to manufacturing and the aforementioned action effects deformation occurs that leads to slope deviations (SD). These deviations represent the difference in the gradient between an ideal undisturbed paraboloid and the actual deformed shape. To assess the accuracy of solar thermal reflectors, the root mean square (RMS) has become established. For the Stellio heliostat, this value is assessed to $SDrms = 1.25\,\mathrm{mrad}$ [26], which serves here as a limit value for the design. Since this limit value applies to an already fully assembled collector, i.e. inaccuracies of the support structure and the mirrors are considered superimposed. A reduced limit value is determined for the grillage only. This is based on the approach of a quadratic mean value from the slope deviation due to the concrete structure $SDrms_{cs}$ and the mirror facets $SDrms_m$. For an equally weighted approach, the limiting value is derived to $SDrms_{cs} = 0.88\,\mathrm{mrad}$. The limitation of the tensile stresses ensuring an uncracked state serves as an additional constraint.

$$SDrms = \sqrt{SDrms_{cs}^2 + SDrms_m^2} \leq 1.25\,\mathrm{mrad} \tag{8}$$

2.6. Structural design using symmetry reduction methods

Due to the circular basic shape of the concrete heliostat, symmetry reduction techniques [42] can be used for pre-design. This allows rotationally symmetric sections of equal modules to be derived. Due to the large focal length – in comparison to PTC – of heliostats, negligible

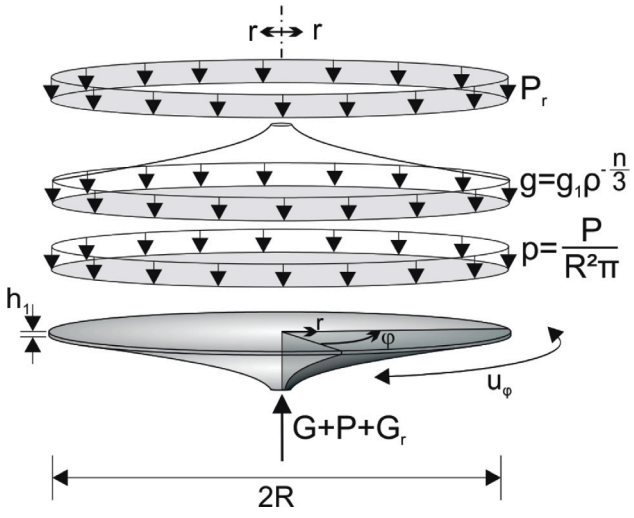

Fig. 3. Rotationally symmetrical plate with hyperbolical thickness, loads and partial structure defined by the angle φ.

curvature results. Additionally, due to the dominant self-weight of concrete structures, the decisive load situation occurs in a horizontal stow position. In consequence, the heliostat can be idealized as a circularly symmetric plate with point-like support at center (Fig. 3). This plate is then designed as an equivalent cantilever arm according to [43] with a length corresponding to the radius R. The plate or cantilever arm, respectively, exhibits a hyperbolic height depending on the unit length $\rho = r/R$ and the edge height h_1:

$$h(\rho) = h_1 \rho^{-n/3} \tag{9}$$

Herein, n is a shape coefficient that determines the curvature of the hyperbolic course and is set to 1.5. Depending on the course of the height and the size of a modular segment – defined by the angle φ – the course of the stiffness as the moment of inertia I_r of a rotationally symmetric plate section can be determined to:

$$I_r = \frac{1}{12} R h_1^3 \rho^{(1-n)} \varphi \tag{10}$$

With respect to φ, the course of the height h can be calculated by means of h_1 in a way that the accuracy demands are fulfilled. Therefore, the loads are simplified according to Fig. 3 to a uniform area load p of 0.5 kN/m^2, representing wind loads and mirror elements, the self-weight of the plate g, defined by the plate's thickness h and its bulk density ρ_c, and a circular line-like load P_r of 0.25 kN/m representing the outer ring. Based on the stiffness I_r, the deformations v can be determined and transferred into slope deviations SD that are the gradients here (Fig. 4a). Then, the height h_1 is searched for so that the resulting $SDrms$ corresponds to the limit value of $SDrms_{cs} = 0.88$ mrad (without inaccuracies of mirrors). The resulting height h is shown in Fig. 4b (black line). Based on Eq. (10) the equivalent stiffness is determined for $\varphi = 90°$ (red line). Thereby, the concentrator consists of 4 modules. To derive the grillage, a beam with a constant width of 10 cm is derived that possesses the same stiffness as a quarter plate. Its resulting height h_{beam} is also shown (green line). The region, where the inner steel ring of the central bearing is located, is greyed out.

For manufacturing, the cross-section height of the radial beams is linearized, tapering from 23 cm at the inner ring to 5 cm at the outer edge. Due to the segmentation into modules, which takes place along the radial struts, the modules have two radial beams with a width of 5 cm each (cf. Fig. 1). Based on Finite-Element (FE) analyses, the secondary struts as well as the outer and inner rings are dimensioned in addition to the radial struts. Thereby, the secondary struts serve as additional support for the mirror elements, which are also considered here as structural parts. The pattern of these struts is derived in a way to minimize mirror deformations using structural optimization [44–46]. The FE analysis uses linear-elastic material behavior since the stresses are limited to the concrete's tensile strength. Moreover, the loads are considered as described in Section 2.4. Hereby, operational and survival states are considered. However, in operational state, both the limiting axial tensile strength f_{ct} and the accuracy demands must be fulfilled. Hereby, the accuracy is limited to $SDrms = 1.25$ mrad since now also deformations of the mirror elements are taken into account. In survival state, the design is restricted by the tensile stresses only. The resulting dimensions of the struts are summarized in Table 3 for which the restrictions are complied with. The individual modules exhibit a weight of approx. 85 kg, so that the concrete grillage alone weighs only about 340 kg. This corresponds to an averaged weight of 42 kg/m^2 for a mirror surface of 8.04 m^2 implying a mean thickness of the concrete structure of 1.8 cm. In comparison, a heliostat with sandwich facets, as described in [47], has a concentrator weight of approximately 12.5 kg/m^2 for a similar mirror surface of around 8 m^2. The Stellio with a mirror area of about 50 m^2 possesses a concentrator weight of about 18 kg/m^2. Despite the slender design of the concrete structure, it still results in higher weight compared to established systems. Generally, the weight of the structure indicates primarily the material used and is therefore a measure of cost, particularly for high production rates. The dimensioning of the drive system is also influenced by the self-weight of the structure, as additional moments from unintended eccentricities of the concentrator must be absorbed by the drive. However, the foundation could even benefit from a heavier concentrator. If vertical loads from the structure outweigh horizontal wind loads, simpler spread foundations rather than more expensive pile foundations might be sufficient.

Table 3
Dimensions of the struts.

Description	Width [cm]	Height [cm]
Radial beam	10 (2 · 5)	23–5
Inner ring	5	23
Outer ring	5	5
Secondary struts	4	4

For robustness and ductile behavior of the concrete structure, additional reinforcement is needed. Therefore, steel rebars with a diameter of 8 mm are chosen. The design of the reinforcement complies to the verification concept of bearing capacity (so-called *ultimate limit state*, ULS) for concrete structures according to European standards [48].

In total, a concrete volume of around 0.14 m^3 is needed for the concentrator. Thus, the material costs can be roughly estimated to about 600 €/m^3. With respect to the mirror area, this results in 10.44 €/m^2. In comparison, the costs for the mirror supporting structure of the Stellio heliostat system are 6.79 $/m^2 while for the SunRing heliostat system they are 8.11 $/m^2 [49]. It must be noted that the cost assumption is cursory, since additional costs, e.g. from the formwork, mirrors, drives and assembly, are not yet included. However, the costs of the concrete collector are close to those of already established heliostat systems.

Based on the amount of material used, the carbon footprint can be derived. For the concrete structure a GWP of 64.4 kg CO_{2e} results according to Table 1. When considering the reinforcement, it is still only 74.6 kg CO_{2e}. In addition, one of the main advantages of the modular design presented here is that individual modules can be replaced rather than dismantling the entire collector when damage occurs or to extend the service life. Thereby, less concrete waste makes it a sustainable design. At the end of the service life, reinforced concrete is typically crushed. The aggregates are then used for recycle concrete or serve as filling material in road construction, which can be categorized as downcycling of material. In contrast, the reinforcing steel can be reused structurally after it has been melted and reshaped.

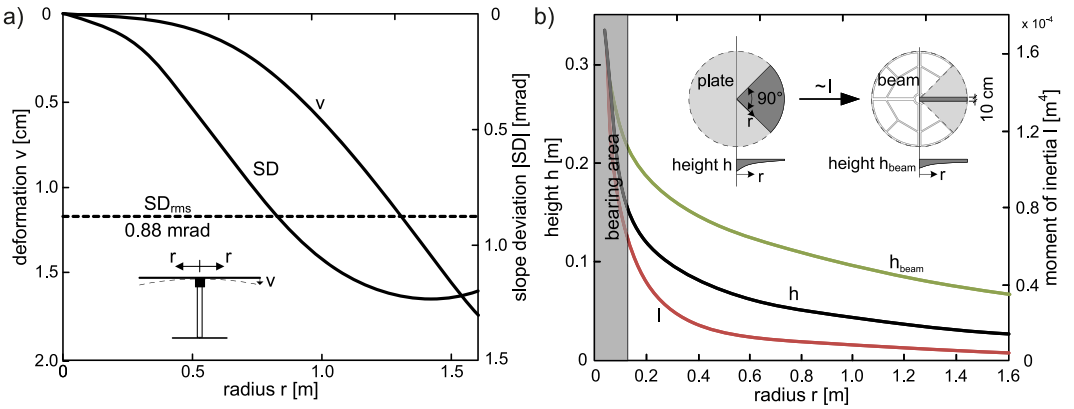

Fig. 4. (a) Deformations v and resulting slope deviations SD for a plate; (b) Thickness of the plate (black) with corresponding moment of inertia (red) and resulting cross-section height of a stiffness-equivalent beam (green). (For interpretation of the references to colour in this figure legend, the reader is referred to the web version of this article.)

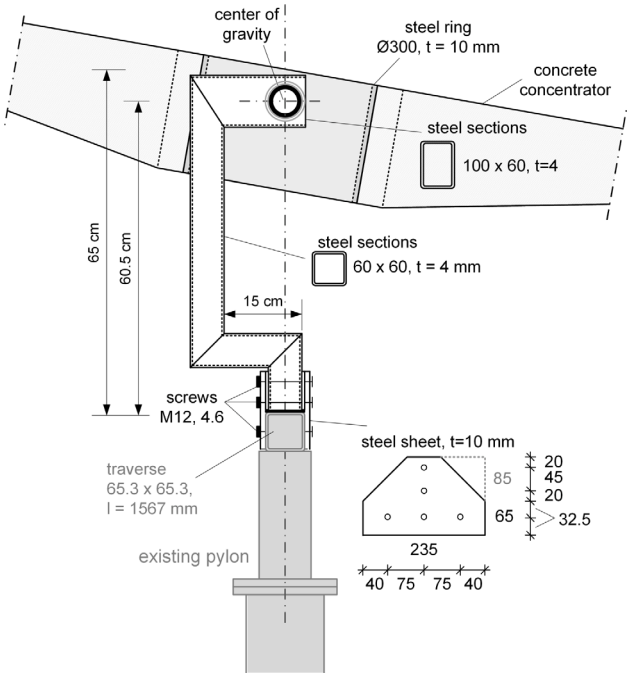

Fig. 5. Detail of the additional support in side-view.

2.7. Design of the bearing

The concrete concentrator is to be erected on an existing pylon from the solar tower at the German Aerospace Center (DLR) in Jülich. For this purpose, two additional C-shaped suspensions made from steel profiles of type S235 were designed on top of the pylon's existing traverse. Thereby, a deflection of up to 30° is enabled without any collision. The construction sketch with measures is shown in Fig. 5.

3. Manufacturing and construction of a prototype

3.1. Manufacturing of the concentrator

The concrete concentrator was manufactured in full-scale in the laboratory of structural engineering at the University of Kaiserslautern-Landau (RPTU). Afterwards, the heliostat was assembled on the HeliTep (Heliostat Testing Platform) at the solar tower Jülich for quality control.

The four concrete modules were produced using a polystyrene formwork multiple times. To secure a safe stripping of the filigree concrete elements, the formwork consisted of five modular parts. These are one main element to ensure the basic grillage structure, one curved part for the outer ring, two side parts for the radial beams, and one inner part for the inner concrete ring. To reduce the adhesion between the polystyrene and the HPC, the surface was covered with epoxy resin layers. For concreting, the assembled formwork parts were fixed with magnets on a production table originating from the production of precast concrete components. To secure the positions of the concrete modules to each other while assembling, three holes were added for the connection of the adjacent radial beams. For the holes, plastic tubes with a diameter of 20 mm were integrated into the formwork. Additionally, a tongue-and-groove joint was milled into the formwork for interlocking the neighboring radial beam's positions (cf. Fig. 6, left).

To avoid collapse in case of unintended, local cracking, reinforcement was considered due to the design in ULS. Therefore, reinforcing steel (type B500 with a characteristic yield strength of $f_{yk} = 500\,\text{MPa}$) and a diameter of 8 mm was used. In the outer ring as well as in the secondary struts one rebar was centrally placed. In the radial beams and inner ring two bars are positioned at the upper and lower edges with a continuous concrete cover of 1 cm, which is sufficient as a protective layer against corrosion for the used HPC. Therefore, a three-dimensional frame for each module was welded together. Additionally to the rebars, micro reinforcement with a diameter of 1 mm and spacings of 1.25 cm was applied between the two reinforcement bars of the radial beam and close to the surfaces in every strut. This stops the propagation of unintended cracks almost directly at the surface. Two of the four modules were constructed with an additional notch in the inner ring to allow the steel tube for the tilting axis to pass through. For the assembly of the concrete concentrator and the installation of the mirror facets, transport anchors were placed at each crossing point of the struts (cf. Fig. 6, right).

Since all modules were produced by only one formwork, the four modules were poured after another. After a hardening time of at least 2 days, the concrete modules were stripped off and the formwork was prepared for the next module. During the manufacturing of the modules, damage to the formwork occurred due to the high adhesion forces of the HPC. For industrial production, a true-to-form steel formwork is hence highly recommended which can be additionally heat treated for reduced stripping times of a few hours only [50,51].

3.2. Substructure and tracking concept

The substructure of the heliostat was realized using a steel pylon from a former steel heliostat of the solar tower Jülich. On top of this pylon a traverse with a rotatable bearing between both, pylon and traverse, was installed. Attached to the traverse two specially manufactured C-shaped suspensions were mounted. At the top end of the suspensions two opposing holes for the horizontal tilting axis of the

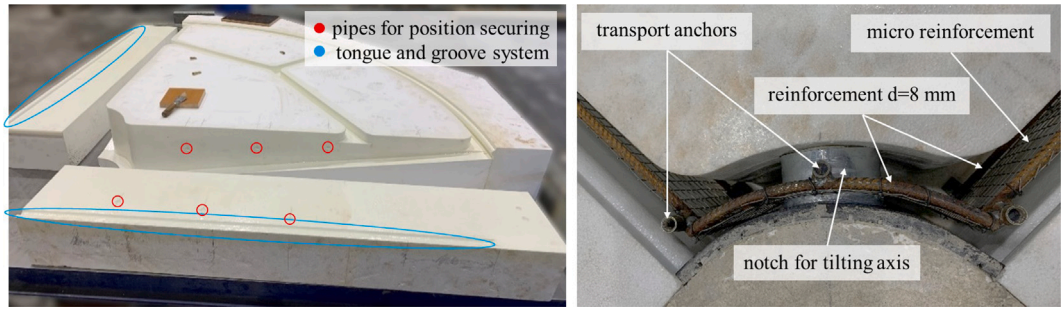

Fig. 6. Detail of the modular formwork with tubes for position securing and tongue and groove system (left), detail of the inner ring with transport anchors and notch for the tilting axis (right).

heliostat were provided (cf. Fig. 7). The tilting axis that connects the bearing with the concrete heliostat consists of a steel tube.

The four concrete modules are connected to a centered steel ring with a diameter of 30 cm, a height of 23 cm, and a thickness of 1 cm (cf. Fig. 7). In addition, this central steel ring has additional stiffeners and a tube that passes horizontally through the steel ring. This horizontal tube is designed in a way that the steel tube of the tilting axis fits exactly to enable tilting. The concentrator can be assembled on the ground and then lifted as a whole. Afterwards, the concentrator and the substructure can be connected by passing through the tilting axis.

For the tracking concept, two linear actuators adapted from the former steel heliostat are used. One is installed horizontally on the pylon and the traverse for rotating the heliostat. For the intended research on the concrete heliostat no specific rotation is needed and this linear actuator was mainly used as fixation. For tilting, the second linear actuator is fixed on the traverse and one of the lower radial beams. Fig. 7 shows both, the horizontal actuator for rotation (colored red) and the vertical actuator for tilting (colored yellow).

3.3. Assembly of the prototype

The full-scale prototype was assembled on the HeliTep at the solar tower Jülich for quality control. First, the four concrete modules were placed around the central steel ring for alignment. Thereby, the circular structure of the concrete heliostat was formed. Afterwards, each module was screwed with the centered steel ring. Additionally, the adjacent radial beams were connected using threaded rods for positioning. To circumvent local stress peaks due to unintended inaccuracies on the radial beam surfaces, an additional layer of elastomer was fixed between the concrete surfaces. After mounting the concrete modules, their upper surfaces were prepared for the mirror facets. Therefore, the contact surfaces of the concrete modules as well as mirror facets were glued using elastomer strips to increase the surface adhesion. On each concrete module, two mirror facets were assembled. Each mirror facet was clamped on the concrete modules simply by stainless steel sheets that were screwed using the provided transport anchors in the grillage (cf. Fig. 6, right).

During assembly of the concentrator, the substructure was erected. Therefore, the pylon was screwed on the existing foundation, and the two C-shaped suspensions on the traverse. Subsequently, the traverse with the C-shaped suspensions and the rotatable bearing were attached on top of the pylon. Afterwards, the concrete concentrator was lifted onto the substructure. Therefore, the holes for the tilting axis of the C-shaped suspensions and the central steel ring were aligned. The connection of the heliostat and the lower construction was realized using a steel tube defining the tilting axis and secured using splints. Then, the vertical linear actuator was screwed to the traverse and fixed using a specially manufactured steel sheet to a threaded rod of the lower radial beam. Finally, the horizontal linear actuator was installed on the pylon and screwed to the traverse. Fig. 8 shows the assembled heliostat with already installed target points on the mirror facets for the photogrammetric quality control.

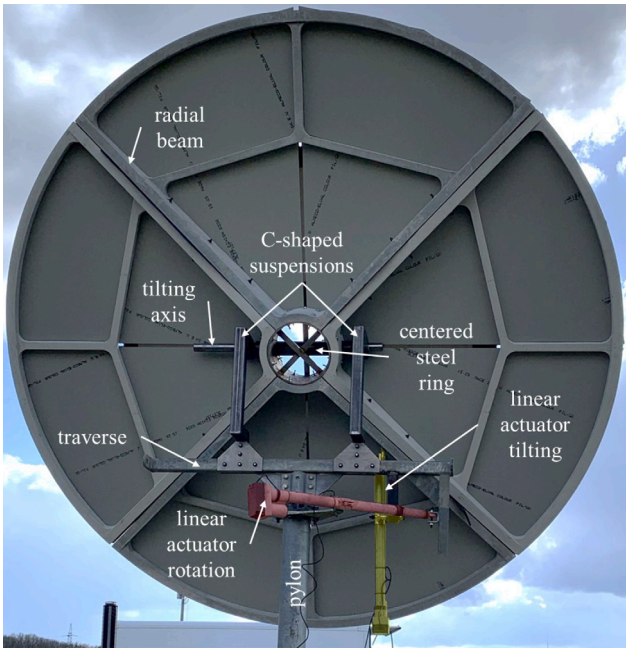

Fig. 7. Back view of the concrete heliostat with detail of the bearing and tracking concept. (For interpretation of the references to colour in this figure legend, the reader is referred to the web version of this article.)

4. Qualification

4.1. Photogrammetric measurement of the mirror surface

For the evaluation of the optical accuracy, the concrete collector is qualified by means of close-range photogrammetric measurement [52, 53] conducted by the German Aerospace Center. Therefore, up to 480 retroreflective targets, around 60 targets per mirror facet, were attached to the mirror surface (cf. Fig. 8). Measurements were taken in different positions with respect to the daily course of the sun. These are the 90°- (stow position), 75°-, 45°-, and 30° position (close to horizon). However, for the stow position maximum deflection occurred as shown

Fig. 8. Front view of the assembled concrete heliostat on the HeliTep at the solar tower Jülich (Germany).

in Fig. 9 (left). The deformations vary between ±10 mm from the ideal shape with respect to the focal length. Based on these deformations, the resulting slope deviations in x- (SDx, center) and y-direction (SDy, right) are calculated, which mainly vary in the range of ±15 mrad. In addition, the RMS-value for each facet is also given. As a result, the total accuracy of $SDrms = 7.8$ mrad could be evaluated. So, the desired accuracy of ≤ 1.25 mrad is not achieved. The individual mirror facets show high differences, which indicate initial rigid body motions meaning inaccuracies in the fastening concept of the mirror facets.

The dimensional stability characterized by the differences in deformation between the individual positions, was further assessed. Deformations observed for the 90° position were used as a reference and deviations from this reference were calculated for the other positions. This means, the deviations for the 90° position vanish. Fig. 10 illustrates the differences in their local z-directions. They increase with decreasing deflection of the concentrator to an almost vertical position of 30°. These deformations are a superposition of structural and mirror deformations with a variation range of approx. ±2 mm. The largest deviations of around −2 mm occur for the 30° deflection, specifically at the edges of two mirror facets each. Hence, these deviations are attributed to local inaccuracies of the mirrors. Thus, it can be inferred that the actual concrete grillage already has high dimensional stability, which is sufficient to maintain the optical effectiveness of the collector during operation.

4.2. Photogrammetric measurement of the concrete structure

For a more detailed evaluation of the concrete modules' geometry, the modules are also photogrammetrically measured in the lab of the Ruhr University Bochum after dismantling the collector on the solar field. In contrast to the mirror qualification, measurement and evaluation were performed using a different, but comparable hardware system and evaluation method. The modules, without mirror facets, were attached to the inner ring in stow position. After removing the glued elastomer strips, measuring targets are placed along the struts on the upper surface at intervals of approximately 10 cm, resulting in about 80 target marks per module.

Fig. 11 displays the vertical downward deformations Δz of the four modules represented as point-wise deformations of the targets and bar plots with corresponding RMS-values for each module. These deformations are attributed to bending of the grillage under dead loads and initial inaccuracies of the concrete elements. The bending deformations increase from the inner fixing (≈ 0) to the outer ring to a maximum of 0.6 mm.

To assess the concreting accuracy, the variations of the measured deformations were evaluated. Maximum deviations result in ±4 mm that, however, only occur for module 2, most likely due to the repeated use and damage of the polystyrene formwork, as previously noted. Nevertheless, the deformations of the other modules mostly vary in the range of ±1 mm. Module 4 possesses slightly higher deviations of up to ±2 mm. The RMS-value – neglecting module 2 – lies in the range of 0.48 (module 3) to 0.91 mm (module 4). These deviations can be explained by the production process as well as by adhesive residues of the elastomer stripes on the surface. Additional grinding could further enhance the accuracy.

5. Conclusions

The conceptual and analytical derivation as well as the construction and optical qualification of a modular concrete heliostat is presented. The main findings are:

- A prototype was developed with an aperture area of 8.04 m^2. The concrete concentrator exhibits an average weight of 42 kg/m^2 with respect to the mirror area which corresponds to only 1.8 cm of concrete if built as a flat disc. Due to its optimized, slender design, a central bearing in the center of gravity without a counterweight – as it was necessary for an already built concrete heliostat – is possible. However, in future research also an individual bearing and tracking concept must be developed for this specific application.
- Due to the modularization, the concentrator structure is segmented into equal modules. These modules are manufactured using a single, modular formwork made from polystyrene. For serial production that becomes necessary for CST plants, reusable and dimensionally stable formworks made from steel, along with incorporated quality management, is sought to ensure the accuracy demands for solar concentration. Initial costs for the formworks would amortize through multiple use. It must be noted that these costs must be analyzed in detail in future investigations with industrial partners.
- The optical qualification is done by photogrammetric measurement. The concrete structure reveals main deformations in the range of ±1 mm including deformations under dead load which indicate remarkable stiffness. In contrast, the qualification of the mirror facets reveals a relatively high slope deviation of $SDrms = 7.8$ mrad, which can be tracked back to the simple and non-adjustable fastening of the mirrors. In future developments, the fastening concept must therefore be improved, but was not the focus here. The measurements presented serve as a benchmark and can be used to validate future work.

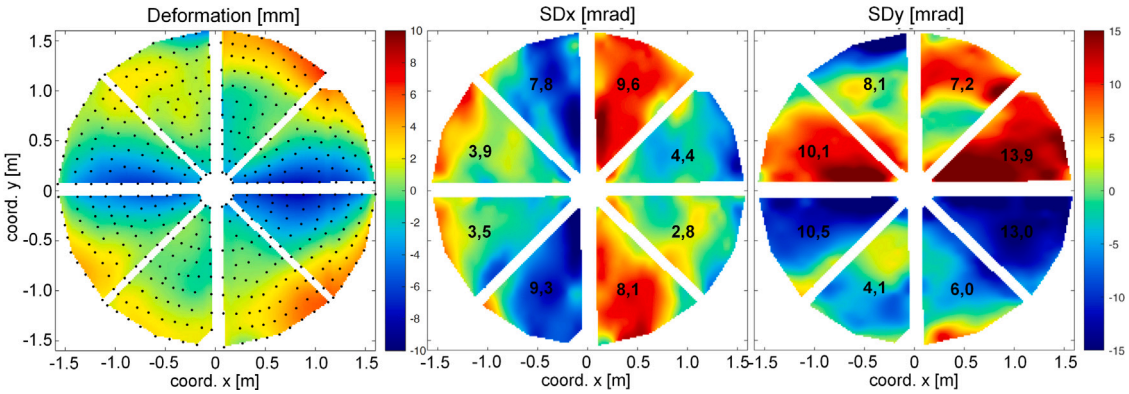

Fig. 9. Measured deformations of the mirror surface in 90° position (left) with corresponding slope deviations SDx (center) and SDy (right) compared to an ideal parabolic shape.

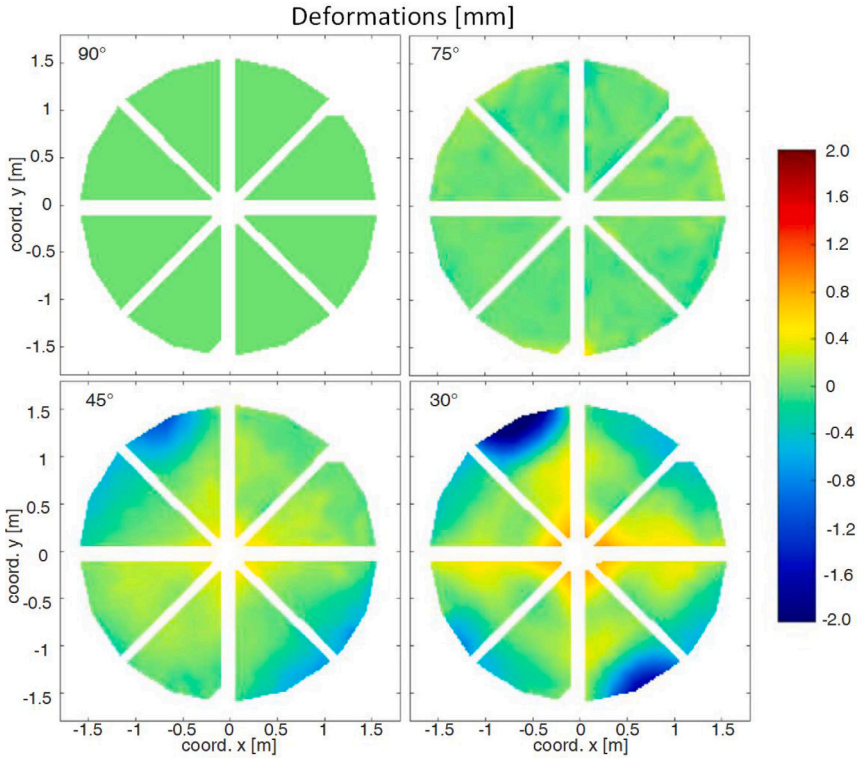

Fig. 10. Differences of the deformations for the 90°, 75°, 45°, and 30° position with respect to 90° position.

- The form stability analysis based on different collector deflections however underlines the stiffness of the concrete structure due to deviations of max. ±2 mm which only occur for local mirror deformations. A concrete concentrator structure has been therefore developed that possesses both high stiffness and low weight. It must now be adapted for larger structures, when integrating cost analysis in the design process.
- The modular design has the additional advantage that single modules can be replaced if damage occurs. This enhances the overall service life without requiring demolition of the whole heliostat, making it a more sustainable design. However, at the end of its service life, the HPC can be recycled like NC and used as aggregates for new (recycling) concrete or in other construction fields as filling. The proposed reinforced concrete structure exhibits a GWP of about 74.6 kg CO_{2e}.
- A cursory cost calculation of the concrete structure mainly considering the materials results in about 10.44 €/m^2, which is in the range of other collector types proposed so far. However, in future investigations detailed cost analysis must be performed corresponding to future developments of the structure to make a valid statement regarding cost efficiency.

A concrete heliostat is structurally feasible, but significant advancements are still needed to address existing research gaps and make it a competitive alternative to current steel-based CST collectors in terms of efficiency and costs. Key areas for development include adapting the design for larger apertures, devising a bearing and tracking system that accommodates the higher dead load of the concrete structure, and conducting a comprehensive cost and efficiency analysis incorporating production and assembly. So far, the developments were focused on technical feasibility of the concentrator structure made from concrete.

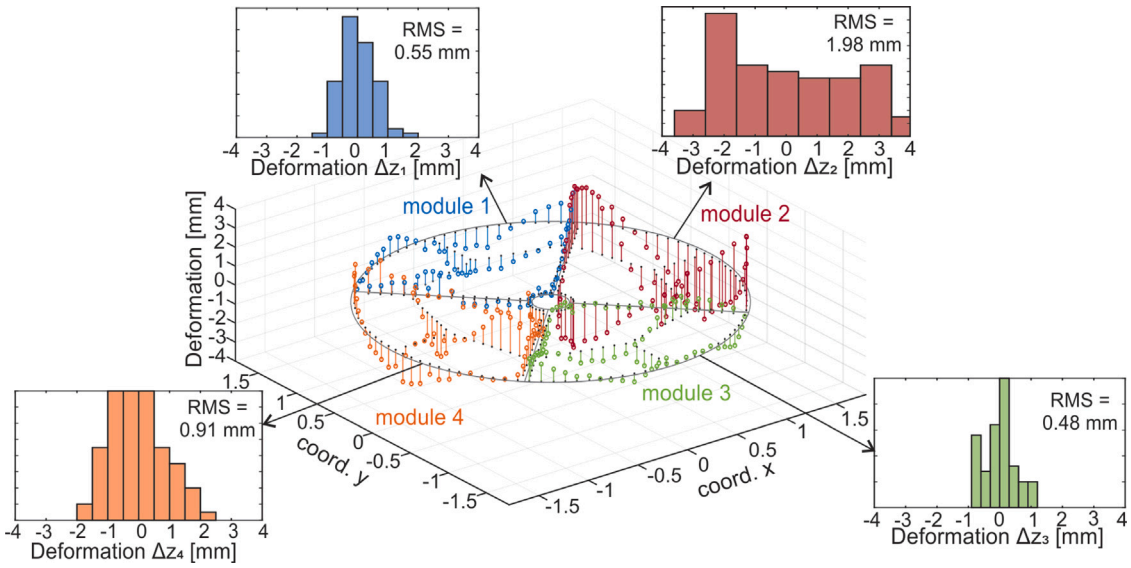

Fig. 11. Deformations Δz of the grillage in the 90° position.

CRediT authorship contribution statement

Patrick Forman: Writing – review & editing, Writing – original draft, Visualization, Validation, Methodology, Investigation, Formal analysis, Conceptualization. **Marius Schellen:** Writing – review & editing, Writing – original draft, Visualization, Validation, Methodology, Investigation, Formal analysis, Conceptualization. **Tim Schlichting:** Writing – review & editing, Visualization, Validation, Investigation. **Andreas Pfahl:** Writing – review & editing, Investigation, Formal analysis. **Peter Mark:** Writing – review & editing, Supervision, Funding acquisition. **Christian Glock:** Writing – review & editing, Supervision. **Jürgen Schnell:** Writing – review & editing, Supervision, Funding acquisition.

Declaration of competing interest

The authors declare that they have no known competing financial interests or personal relationships that could have appeared to influence the work reported in this paper.

Acknowledgments

This work was supported by the German Research Foundation [grant number 389020360]. The authors like to thank their project partners, especially Dr.-Ing. habil. Bernhard Sagmeister (Durcrete GmbH), Dipl.-Ing. Thomas Friedrich (Innogration GmbH) and Dr. rer. nat. Reinhard Dasbach (Almeco GmbH).

References

[1] SolarPACES, CSP projects around the world, 2022 https://www.solarpaces.org/csp-technologies/csp-projects-around-the-world/, (Accessed 13 December 2022).
[2] C. Glock, M. Heckmann, T. Hondl, F. Kaufmann, M. Schellen, R. Sefrin, Solid construction in times of climate change and resource scarcity - challenges and solutions [in German], Bauingenieur 97 (01–02) (2022) 1–12, http://dx.doi.org/10.37544/0005-6650-2022-01-02-33.
[3] A.B. Awan, M. Zubair, R.P. Praveen, A.R. Bhatti, Design and comparative analysis of photovoltaic and parabolic trough based CSP plants, Sol. Energy 183 (2019) 551–565, http://dx.doi.org/10.1016/j.solener.2019.03.037.
[4] D.A. Baharoon, H.A. Rahman, W.Z.W. Omar, S.O. Fadhl, Historical development of concentrating solar power technologies to generate clean electricity efficiently – A review, Renew. Sustain. Energy Rev. 41 (2015) 996–1027, http://dx.doi.org/10.1016/j.rser.2014.09.008.
[5] W. Fuqiang, C. Ziming, T. Jianyu, Y. Yuan, S. Yong, L. Linhua, Progress in concentrated solar power technology with parabolic trough collector system: A comprehensive review, Renew. Sustain. Energy Rev. 79 (2017) 1314–1328, http://dx.doi.org/10.1016/j.rser.2017.05.174.
[6] R.P. Merchán, M.J. Santos, A. Medina, A. Calvo Hernández, High temperature central tower plants for concentrated solar power: 2021 overview, Renew. Sustain. Energy Rev. 155 (2022) 111828, http://dx.doi.org/10.1016/j.rser.2021.111828.
[7] A. Pfahl, J. Coventry, M. Röger, F. Wolfertstetter, J.F. Vásquez-Arango, F. Gross, M. Arjomandi, P. Schwarzbözl, M. Geiger, P. Liedke, Progress in heliostat development, Sol. Energy 152 (2017) 3–37, http://dx.doi.org/10.1016/j.solener.2017.03.029.
[8] A. Pfahl, Survey of heliostat concepts for cost reduction, J. Solar Energy Eng. 136 (1) (2014) http://dx.doi.org/10.1115/1.4024243.
[9] J. Coventry, J. Pye, Heliostat cost reduction – where to now? Energy Procedia 49 (2014) 60–70, http://dx.doi.org/10.1016/j.egypro.2014.03.007.
[10] K.R. Bhargav, F. Gross, P. Schramek, Life cycle cost optimized heliostat size for power towers, Energy Procedia 49 (2014) 40–49, http://dx.doi.org/10.1016/j.egypro.2014.03.005.
[11] J. Weissert, Y. Zhou, D. You, H. Metghalchi, Current advancement of heliostats, J. Energy Resour. Technol. 144 (12) (2022) http://dx.doi.org/10.1115/1.4054738.
[12] A. Belaid, A. Filali, A. Gama, B. Bezza, T. Arrif, M. Bouakba, Design optimization of a solar tower power plant heliostat field by considering different heliostat shapes, Int. J. Energy Res. 44 (14) (2020) 11524–11541, http://dx.doi.org/10.1002/er.5772.
[13] A. Belaid, A. Filali, S. Hassani, T. Arrif, M. Guermoui, A. Gama, M. Bouakba, Heliostat field optimization and comparisons between biomimetic spiral and radial-staggered layouts for different heliostat shapes, Sol. Energy 238 (2022) 162–177, http://dx.doi.org/10.1016/j.solener.2022.04.035.
[14] V. Grigoriev, K. Milidonis, C. Corsi, M. Blanco, Heliostat fields with a balanced mirror density, Sol. Energy 243 (2022) 336–347, http://dx.doi.org/10.1016/j.solener.2022.07.050.
[15] N. Nedaei, F. Hamrang, L.G. Farshi, Design and 3E analysis of a hybrid power plant integrated with a single-effect absorption chiller driven by a heliostat field: A case study for Doha, Qatar, Energy 239 (2022) 122415, http://dx.doi.org/10.1016/j.energy.2021.122415.
[16] M. Gadalla, M. Saghafifar, A concise overview of heliostat fields-solar thermal collectors: Current state of art and future perspective, Int. J. Energy Res. 42 (10) (2018) 3145–3163, http://dx.doi.org/10.1002/er.4041.
[17] C.K. Ho, B.D. Iverson, Review of high-temperature central receiver designs for concentrating solar power, Renew. Sustain. Energy Rev. 29 (2014) 835–846, http://dx.doi.org/10.1016/j.rser.2013.08.099.
[18] R. Angel, R. Eads, N. Didato, M. Rademacher, N. Emerson, C. Davila, Actively shaped focusing heliostat, AIP Conf. Proc. 2445 (2022) 120003, http://dx.doi.org/10.1063/5.0086409.
[19] A. Pfahl, A. Rong, Low-cost movable heliostat, AIP Conf. Proc. 2445 (2022) 120019, http://dx.doi.org/10.1063/5.0086923.
[20] M. Yang, Y. Zhang, Q. Wang, Y. Zhu, R.A. Taylor, A coupled structural-optical analysis of a novel umbrella heliostat, Sol. Energy 231 (2022) 880–888, http://dx.doi.org/10.1016/j.solener.2021.12.018.

[21] P. Forman, S. Müller, M.A. Ahrens, J. Schnell, P. Mark, R. Höffer, K. Hennecke, J. Küger, Light concrete shells for parabolic trough collectors – conceptual design, prototype and proof of accuracy, Sol. Energy 111 (2015) 364–377, http://dx.doi.org/10.1016/j.solener.2014.11.002.

[22] M. Emes, A. Jafari, A. Pfahl, J. Coventry, M. Arjomandi, A review of static and dynamic heliostat wind loads, Sol. Energy 225 (2021) 60–82, http://dx.doi.org/10.1016/j.solener.2021.07.014.

[23] M.J. Emes, M. Arjomandi, G.J. Nathan, Effect of heliostat design wind speed on the levelised cost of electricity from concentrating solar thermal power tower plants, Sol. Energy 115 (2015) 441–451, http://dx.doi.org/10.1016/j.solener.2015.02.047.

[24] U. Winkelmann, C. Kämper, R. Höffer, P. Forman, M.A. Ahrens, P. Mark, Wind actions on large-aperture parabolic trough solar collectors: Wind tunnel tests and structural analysis, Renew. Energy 146 (2020) 2390–2407, http://dx.doi.org/10.1016/j.renene.2019.08.057.

[25] T. Keck, V. Schönfelder, B. Zwingmann, F. Gross, M. Balz, F. Siros, G. Flamant, High-performance stellio heliostat for high temperature application, in: SOLARPACES 2020: 26th International Conference on Concentrating Solar Power and Chemical Energy Systems, in: AIP Conference Proceedings, AIP Publishing, 2022, 120014, http://dx.doi.org/10.1063/5.0086592.

[26] M. Balz, V. Göcke, T. Keck, F. von Reeken, G. Weinrebe, M. Wöhrbach, Stellio – development, construction and testing of a smart heliostat, AIP Conf. Proc. 1734 (2016) 020002, http://dx.doi.org/10.1063/1.4949026.

[27] A. Pfahl, F. Gross, P. Liedke, J. Hertel, J. Rheinländer, S. Mehta, J.F. Vásquez-Arango, S. Giuliano, R. Buck, Reduced to minimum cost: Lay-down heliostat with monolithic mirror-panel and closed loop control, AIP Conf. Proc. 2033 (2018) 040030, http://dx.doi.org/10.1063/1.5067066.

[28] A.A. Rizvi, S.N. Danish, A. El-Leathy, H. Al-Ansary, D. Yang, A review and classification of layouts and optimization techniques used in design of heliostat fields in solar central receiver systems, Sol. Energy 218 (2021) 296–311, http://dx.doi.org/10.1016/j.solener.2021.02.011.

[29] P. Forman, S. Penkert, C. Kämper, T. Stallmann, P. Mark, J. Schnell, A survey of solar concrete shell collectors for parabolic troughs, Renew. Sustain. Energy Rev. 134 (2020) 110331, http://dx.doi.org/10.1016/j.rser.2020.110331.

[30] C. Kämper, P. Forman, T. Stallmann, M.A. Ahrens, P. Mark, J. Schnell, Optimised high-performance concrete shells for parabolic trough collectors, J. Int. Assoc. Shell Spat. Struct. 58 (No. 1 March n. 191) (2017) 105–119, http://dx.doi.org/10.20898/j.iass.2017.191.843.

[31] P. Froman, C. Glock, P. Mark, Fast construction - motivation, history and concepts [in German], Beton- und Stahlbetonbau 116 (Sonderheft 2) (2021) 2–11, http://dx.doi.org/10.1002/best.202100064.

[32] P. Forman, S. Penkert, A. Pfahl, J. Schnell, P. Mark, Development of a modular concrete heliostat prototype, AIP Conf. Proc. 2445 (2022) http://dx.doi.org/10.1063/5.0086016.

[33] P. Forman, S. Penkert, P. Mark, J. Schnell, Design of modular concrete heliostats using symmetry reduction methods, Civ. Eng. Des. 2 (4) (2020) 92–103, http://dx.doi.org/10.1002/cend.202000013.

[34] P. Mark, G. Lanza, D. Lordick, A. Albers, M. König, A. Borrmann, L. Stempniewski, P. Forman, A.M. Frey, R. Renz, A. Manny, J. Stindt, Industrializing precast productions, Civ. Eng. Des. 3 (3) (2021) 87–98, http://dx.doi.org/10.1002/cend.202100019.

[35] DIN EN 196-1:2016-11, Methods of Testing Cement - Part 1: Determination of Strength; German Version EN 196-1:2016, Standard, 2016, http://dx.doi.org/10.31030/2482416.

[36] DIN EN 12390-5:2019-10, Testing Hardened Concrete - Part 5: Flexural Strength of Test Specimens; German Version EN 12390-5:2019, Standard, 2019, http://dx.doi.org/10.31030/3045736.

[37] U. Fischer, "Hochleistungsbeton für Alle": Nanotechnologisch Optimierter, Langlebiger, energieeffizienter und insbesondere AnwendungsFreundlicher Hochleistungsbeton -OLAF-, Technical Report, Evonik Industries AG, 2012.

[38] A. Pfahl, M. Buselmeier, M. Zaschke, Wind loads on heliostats and photovoltaic trackers of various aspect ratios, Sol. Energy 85 (9) (2011) 2185–2201, http://dx.doi.org/10.1016/j.solener.2011.06.006.

[39] H. Sun, B. Gong, Q. Yao, A review of wind loads on heliostats and trough collectors, Renew. Sustain. Energy Rev. 32 (2014) 206–221, http://dx.doi.org/10.1016/j.rser.2014.01.032.

[40] B. Gong, Z. Wang, Z. Li, C. Zang, Z. Wu, Fluctuating wind pressure characteristics of heliostats, Renew. Energy 50 (2013) 307–316, http://dx.doi.org/10.1016/j.renene.2012.06.037.

[41] J.A. Peterka, R. Derickson, Wind Load Design Methods for Ground-Based Heliostats and Parabolic Dish Collectors, Technical Report SAND-92-7009, 1992, http://dx.doi.org/10.2172/7105290.

[42] L. Bocklenberg, P. Mark, Thick slab punching with symmetry reductions, Struct. Concr. 21 (3) (2020) 875–889, http://dx.doi.org/10.1002/suco.201900480.

[43] G. Márkus, Theorie und Berechnung rotationssymmetrischer Bauwerke, 3, Werner, Düsseldorf, 1978.

[44] G. Gaganelis, P. Mark, P. Forman, Optimization Aided Design: Reinforced Concrete, Ernst & Sohn and Wiley, Berlin and Weinheim, 2022.

[45] P. Forman, G. Gaganelis, P. Mark, Optimization-based design [in German], Bautechnik 97 (10) (2020) 697–707, http://dx.doi.org/10.1002/bate.202000054.

[46] G. Gaganelis, P. Mark, Downsizing weight while upsizing efficiency: An experimental approach to develop optimized ultra-light UHPC hybrid beams, Struct. Concr. 20 (6) (2019) 1883–1895, http://dx.doi.org/10.1002/suco.201900215.

[47] A. Pfahl, M. Randt, C. Holze, M. Unterstütz, Autonomous light-weight heliostat with rim drives, Sol. Energy 92 (2013) 230–240, http://dx.doi.org/10.1016/j.solener.2013.03.005.

[48] DIN EN 1992-1-1:2011-01, Eurocode 2: Design of Concrete Structures - Part 1-1: General Rules and Rules for Buildings; German Version EN 1992-1-1:2004 + AC:2010, Standard, 2010, http://dx.doi.org/10.31030/1723945.

[49] P. Kurup, S. Akar, S. Glynn, C. Augustine, P. Davenport, Cost Update: Commercial and Advanced Heliostat Collectors, Technical Report, National Renewable Energy Laboratory (NREL), 2022, URL https://www.nrel.gov/docs/fy22osti/80482.pdf.

[50] J. Stindt, P. Forman, P. Mark, Influence of rapid heat treatment on the shrinkage and strength of high-performance concrete, Materials 14 (15) (2021) 4102, http://dx.doi.org/10.3390/ma14154102.

[51] J. Stindt, P. Forman, P. Mark, Experimente zur Schwindreduktion von hochfesten Betonbauteilen durch Wärmebehandlung, Beton- und Stahlbetonbau 116 (8) (2021) 87–98, http://dx.doi.org/10.1002/best.202100028.

[52] K. Blume, M. Röger, T. Schlichting, A. Macke, R. Pitz-Paal, Dynamic photogrammetry applied to a real scale heliostat: Insights into the wind-induced behavior and effects on the optical performance, Sol. Energy 212 (2020) 297–308, http://dx.doi.org/10.1016/j.solener.2020.10.056.

[53] K. Pottler, E. Lüpfert, G.H.G. Johnston, M.R. Shortis, Photogrammetry: A powerful tool for geometric analysis of solar concentrators and their components, J. Solar Energy Eng. 127 (1) (2005) 94–101, http://dx.doi.org/10.1115/1.1824109.